Applied Catalysis B: Environmental 238 (2018) 302–308

Contents lists available at ScienceDirect

Applied Catalysis B: Environmental

journal homepage: www.elsevier.com/locate/apcatb

Enhanced photocatalytic activity of PTCDI-C_{60} via π–π interaction

Yunxia Wei[a], Mingguang Ma[a], Wenlu Li[b], Jun Yang[b], Hong Miao[b], Zijian Zhang[b], Yongfa Zhu[b,*]

[a] College of Chemistry and Chemical Engineering, Lanzhou City University, Lanzhou 730070, PR China
[b] Department of Chemistry, Tsinghua University, Beijing 100084, PR China

ARTICLE INFO

Keywords:
Photocatalysis
Pollutants degradation
Visible light
π − π interaction

ABSTRACT

The π–π stacking of self-assembled PTCDI and π–π interactions between self-assembled PTCDI and C_{60} result in fast transfer of the photogenerated carriers and reduced carrier recombination. The π–π interaction lowers the position of valence band and narrows the band gap, thus leading to a stronger redox ability and a broad spectral response. The organic photocatalyst PTCDI-C_{60} can not only degrading phenol at a rate of 0.216 h^{-1}, which is 8.24 times higher than that of pure PTCDI, but also producing oxygen at a rate of 22.5 μmol g^{-1} h^{-1}. Moreover, the presence of C_{60} stabilizes the composite to decrease the accumulation of negative charge. The high catalytic activity can potentially be utilized in the fields of environmental and energy applications.

1. Introduction

The π-π interactions are generally defined as the attractive interactions that occur between the π-clouds of aromatic systems in a parallel, face-to-face orientation. It is, in fact, in the absence of spectroscopic evidence for HOMO-LUMO interactions [1]. They play a fundamental role in many aspects of chemistry and biochemistry [2–4], for example in the fields molecular recognition [5], self-assembly [6,7], supramolecular chemistry, and general host-guest interactions [8–11].

Mononuclear complexes containing aromatic ligands can be assembled into various supramolecular architectures by means of π–π interactions of the aromatic rings. It is worth mentioning that the noncovalent interactions lead not only to various supermolecules and solid-state architectures, but generate also interesting supramolecular properties, such as electrical, optical and magnetic ones [12].

Perylene tetracarboxylic diimide (PTCDI), a widely used n-type semiconductor, has attracted much attention because of its outstanding stability, excellent electron affinity, and chargecarrier migration arising from its π–π stacking [13]. On the strength of these properties, many applications have been investigated, such as organic field-effect transistors (OFETs) [14], solar cells [15], photon harvesting [16], sensors [17] and photoswitches [18].

Our group first presented an economical and rapid method to form a self-assembled nanophotocatalyst for the degradation of organic pollutants under visible light, and explained that the band-like electronic energy level structure of the PTCDI supramolecular system originating from orbital overlaps between PTCDI molecular units and long-range conjugated π-delocalization within the self-assembled PTCDI supramolecular system mainly contributes to its remarkable photocatalytic properties [19]. On this basis, we also reported that the TCNQ-PTCDI visible light catalyst, which is composed of PTCDI and TCNQ with a relatively large conjugate system, can formed a high-speed channel, which is advantageous to the separation and migration of photogenic carriers, and disadvantageous to the composite of photogenic electrons and holes because of the π–π interactions between TCNQ and PTCDI [20]. These related researches provide a new way to improve the separation and migration rate of photogenic carriers of organic photocatalyst.

Fullerenes(C_{60}) is an electronegative molecule and suitable for efficient electron transfer because π orbital of C_{60} is more out of the cage and the electronic structure of C_{60} has naturally focused on the surface 30 π-orbitals [21–24]. The symmetry of the C_{60}, the conical alignment of the conjugate large π bond system and the conical alignment of C atoms result in fast electron transfer and slow electron recombination. Photocatalysts/C_{60} have been prepared to improve the performance of photocatalyst [25–27].

On the basis of these concerns, PTCDI will also be able to combine well with C_{60} through strong π-π interaction between conjugated systems. The electrons are transferred through the π–π long-range transport pathway of self-assemble PTCDI and tend to transfer to C_{60}, then they will be transferred through the large π bond using C_{60} as an electronic separation center result in fast transfer of carriers and reduced carrier recombination. The photocatalytic performance of the catalyst will be enhanced.

* Corresponding author.
E-mail address: Zhuyf@mail.tsinghua.edu.cn (Y. Zhu).

https://doi.org/10.1016/j.apcatb.2018.07.043
Received 15 May 2018; Received in revised form 11 July 2018; Accepted 13 July 2018
Available online 19 July 2018

2. Experimental

2.1. Preparation of PTCDI-C_{60} photocatalyst

Perylene tetracarboxylic diimide (PTCDI) was purchased from Sinopharm Chemical Reagent Corp., Beijing, P. R. China. Fullerene(C_{60}) was purchased from Suzhou carbon Feng graphene Technology Co., Ltd. Sulfuric acid was purchased from Beijing Chemical Works. All reagents used in this research were commercially available and used without further purification.

The preparation of PTCDI-C_{60} photocatalysts was as follows: 50 mg C_{60} was dispersed in 100 ml concentrated sulfuric acid under ultrasonication for 5 h to form colloidal. 0.1 g PTCDI was dissolved with 2 mL of concentrated sulfuric acid, the appropriate amount of C_{60} colloidal according to the different mass ratio of the total mass of PTCDI and C_{60} was added into the above solution under ultrasonication for 3 h. The mixture was carefully added dropwise to 50 mL of water under stirring for 3 h, then, dark violet products were precipitated, washed several times. The product was then filtered and dried at 60 °C in a vacuum drying oven. In this way, composite photocatalysts with different C_{60} mass ratios ranging from 0.01% to 30% were synthesized. As shown in the optical photograph presented in Fig. S1, the final products were dark brown with a bit of metal luster before grinding.

2.2. Characterization of PTCDI-C_{60} photocatalyst

The crystallinity of the composites was determined on a Bruker D8 ADVANCE diffractometer under Cu Kα radiation. The structures and morphologies were examined by field-emission scanning electron microscopy (SEM, LEO-1530). High resolution transmission electron microscopy (HRTEM) images were obtained on a JEM 2010 F field-emission gun transmission electron microscope at an accelerating voltage of 200 kV. Atomic force microscopy (AFM) measurements were carried out on an SPM-9700 scanning probe microscope (Shimadzu Corporation). Fourier transform infrared (FTIR) spectra were obtained using a Bruker V70FTIR spectrometer. UV–vis diffuse reflectance spectroscopy (UV-DRS) was performed on a Hitachi U-3010 UV–vis spectrophotometer with $BaSO_4$ as the reference. Raman spectra were obtained with a Horiba JY HR800 confocal microscope Raman spectrometer under an Ar-ion laser (514 nm). The photocurrent was measured on an electrochemical system(CHI-660B). Electron spin resonance (ESR) spectra were recorded from the sample mixture, containing spin-trapping probes such as 5,5- dimethyl-1- -N-oxide(DMPO), 2,2,6,6-tetramethyl-4-piperidone(TEMP), or 2,2,6,6-t pirroline etramethylpiperidine-1-oxyl (TEMPO) and products, after exposure to visible light for selected times using an electron–nuclear double resonance (ENDOR) spectrometer (JEOL ES-ED3X) at room temperature. X-ray photoelectron spectroscopy (XPS) was performed to estimate the VB positions of PTCDI, self-assemble PTCDI and 0.1%-PTCDI-C_{60} using a PHI 5300 ESCA system. PHI Quantera SXMTM system was used to get XPS spectra.

2.3. Photocatalytic evaluation

The photocatalytic degradation of phenol was conducted under visible light (> 420 nm). The light source was a 500-W Xe lamp with a 420-nm cutoff filter, produced by Institute for Electric Light Sources, whose average light intensity was 35 mW cm^{-2}. In the photocatalytic experiments, 25 mg of powder composite photocatalyst was dispersed in an aqueous solution of phenol (50 mL, 5 ppm). Before the light irradiation, the suspensions were stirred in the dark for 1 h to ensure absorption–desorption equilibrium. At intervals of 1 h, aliquots of 2 mL were withdrawn and centrifuged. The concentration of phenol was analyzed by high-performance liquid chromatography (Shimadzu LC-20AT) with UV detection (270 nm). A Venusil XBP-C18 (Agela Technologies Inc.) column was used, and the mobile phase consisted of methanol and pure water (55:45 for phenol, v/v) at a flow rate of 1 mL min^{-1}.

The photocatalytic water oxidation reaction was carried out with a Labsolar-IIIAG system (Perfect Light, Beijing) in the presence of 0.01 mol L^{-1} silver nitrate as an electron acceptor. The photocatalyst powders (50 mg) were added to 100 mL $AgNO_3$(aq) in the reaction cell with a magnetic stirrer. The light source was a 500-W xenon lamp with a 420-nm cutoff filter. The amount of evolved oxygen was determined using a gas chromatograph (GC 7920, thermal conductivity detector, Ar carrier).

2.4. Electrochemical measurement

To investigate the photoelectrochemical performance of the composites, a standard three-electrode cell was employed, with a composite as the working lectrode, a saturated calomel electrode (SCE) as the reference lectrode, and a platinum wire as the counter electrode. Na_2SO_4 was taken as the electrolyte solution. The working electrodes were repared as follows: A composite (5 mg) was suspended in 1 mL of pure/deionized water under grinding and ultrasonication. A dark purple slurry was obtained and dip-coated onto an indium tin oxide (ITO) glass electrode.

3. Results and discussion

3.1. Photocatalytic activity

Fig. 1 presents the photocatalytic activities of the photocatalysts under visible light (> 420 nm) in the degradation of phenol and the oxidation of water. Dramatically, the apparent rate constant of degradation for 5 ppm phenol first rose and then dropped with increasing C_{60} content (see Fig. 1a). When the mass ratio reached 0.1%, the apparent rate constant of degradation reached the maximum of 0.216 h^{-1}, nearly 8.24 times that of pure PTCDI (0.026 h^{-1}), and 2.27 times that of self-assemble PTCDI. However, when the ratio was over 0.1%, the phenol-degradation rate constant decreased notably. Furthermore, the highly efficient 0.1%-PTCDI-C_{60} catalyst could produce

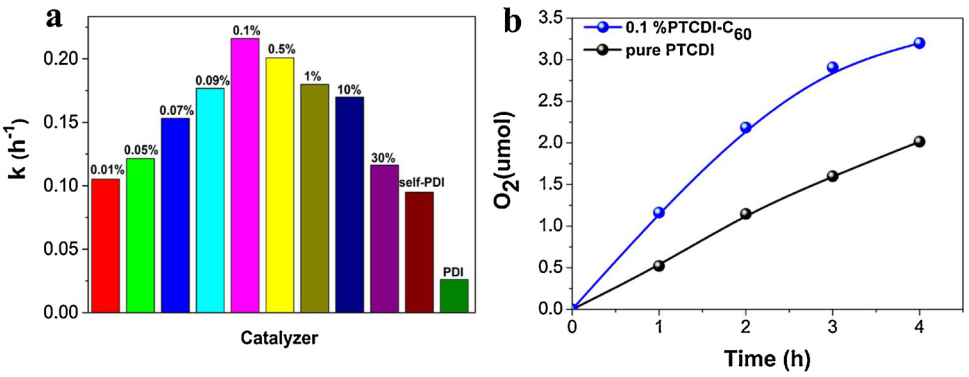

Fig. 1. Photocatalytic activities of PTCDI-C_{60} composite materials: (a) Apparent rate constants k of PTCDI-C_{60} composite photocatalysts for the degradation of 5 ppm phenol with different C_{60} mass ratios under visible light (λ > 420 nm); (b) amount of evolved oxygen in photocatalytic water oxidation with 0.1%-PTCDI-C_{60} under visible light (λ > 420 nm).

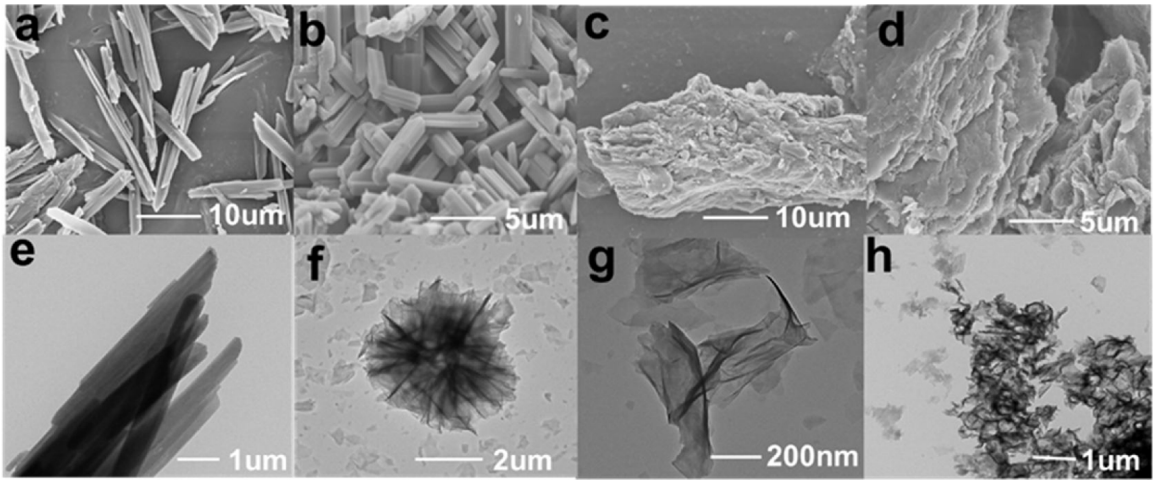

Fig. 2. Morphology-related results for PTCDI-C_{60} composite materials: (a) scanning electron microscopy image of pure PTCDI, (b) scanning electron microscopy image of pure C_{60}, (c) and (d) scanning electron microscopy image of 0.1%-PTCDI-C_{60} composite, (e) transmission scanning electron microscopy image of pure PTCDI, (f) and (g) transmission scanning electron microscopy image of pure C_{60}, (h) transmission scanning electron microscopy image of 0.1%-PTCDI-C_{60} composite.

oxygen from water under visible light, as showed in Fig. 1b, when the light was turned on, the amount of oxygen increased rapidly at a rate of 22.5 μmol g^{-1} h^{-1}, nearly 2 times that of pure PTCDI. At same time, the apparent rate constant of degradation for 5 ppm phenol of several common photocatalysts under the same conditions are also listed in Supporting Information in Table S1.

We were interested in why the 0.1%-PTCDI-C_{60} composite could gain the strongest oxidation ability and why the activity declined when the mass ratio of C_{60} less than or greater than 0.1%.

3.2. π-π interaction enhanced activity of the photocatalyst

The property of a material is determined by its structure. We will explore this problem by observing the morphology of material first, then going deep into its internal structure. The morphology of the PTCDI-C_{60} composite looks like layer-by-layer shale in the SEM images (Fig. 2d). By AFM, the thickness of each layer was detected in the range of 0.15–3 nm (Fig. S4). It can be seen from TEM, the commercial PTCDI shows thick-rod structure whereas 0.1%-PTCDI-C_{60} exhibits the willow leaf-like shape (Fig. 2e and h). It so happened that this shape can provide higher surface active sites [28,29].

In the X-ray diffraction (XRD) image of a series of catalysts (Fig. 3a), the crystalline peaks of C_{60} located at (111), (220), (311), (222) (JCPDS. No. 79-1715) are also detected in PTCDI-C_{60} sample. Obviously, the PTCDI-C_{60} formed an ordered structure and its crystallization property has been enhanced in comparison with pure PTCDI and self-assemble PTCDI, which is beneficial for its enhanced photocatalytic activity. In addition, maybe amount of C_{60} in 0.1-PTCDI-C_{60} is too few to be detected. XRD peaks corresponding to typical π–π stacking distance between the PTCDI perylene skeletons with d-spacing of 3.2–3.7 Å emerged. 3.27 Å can be attributed to closely co-facial π–π stacking distance, whereas 3.27 Å should correspond to distances of π–π stacking interaction between PTCDI molecules adopting twisted arrangements.

In the HRTEM image of 0.1%-PTCDI-C_{60} (Fig. 3b), there are many nanocrystalline PTCDI areas with a d spacing of ~0.36 nm and a diameter of < 10 nm, the directions of the lattice fringes are different depending on the region. In the magnification of the dashed region indicated the d spacing ranges from 0.34 to 0.38 nm, which is normally observed for π–π stacking [30]. On the other hand, the mean free path of photogenerated carriers is about 10 nm; a photocatalyst size of less than 10 nm just is good for photogenerated carriers transferring to the surface and substrate. This is also one of the reasons that nanoscale photocatalysts can gain high efficiency, which makes photogenerated carriers transfer faster and more easily with less chance of recombination.

The FT-IR spectrum of 0.1%-PTCDI-C_{60} supramolecular system is almost the same as that of pure PTCDI (Fig. S2). It was reported that formation of N—H···O hydrogen bonds between the imide hydrogen atoms and the carbonyl oxygen atoms would lead the stretching vibrations of N—H and C=O to lower wavenumbers [31]. Hereby, stretching frequencies at υ(N—H) = 3153, 3034 cm^{-1} and υ(C=O) = 1662 cm^{-1} in this FT-IR spectrum indicate that intermolecular hydrogen bonds form between N—H and C=O groups in pure PTCDI

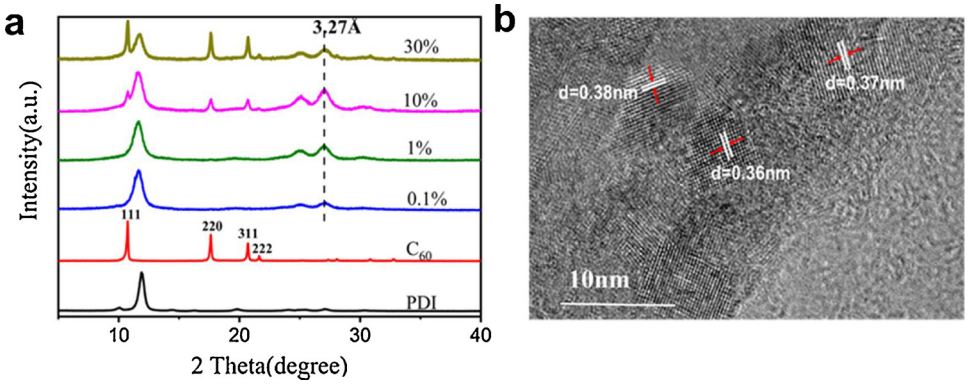

Fig. 3. Structure-related results for PTCDI-C_{60} compositematerials: (a) X-ray diffraction image of PTCDI-C_{60} composite, (b) high-resolution transmission electron microscopy image of 0.1%-PTCDI-C_{60}.

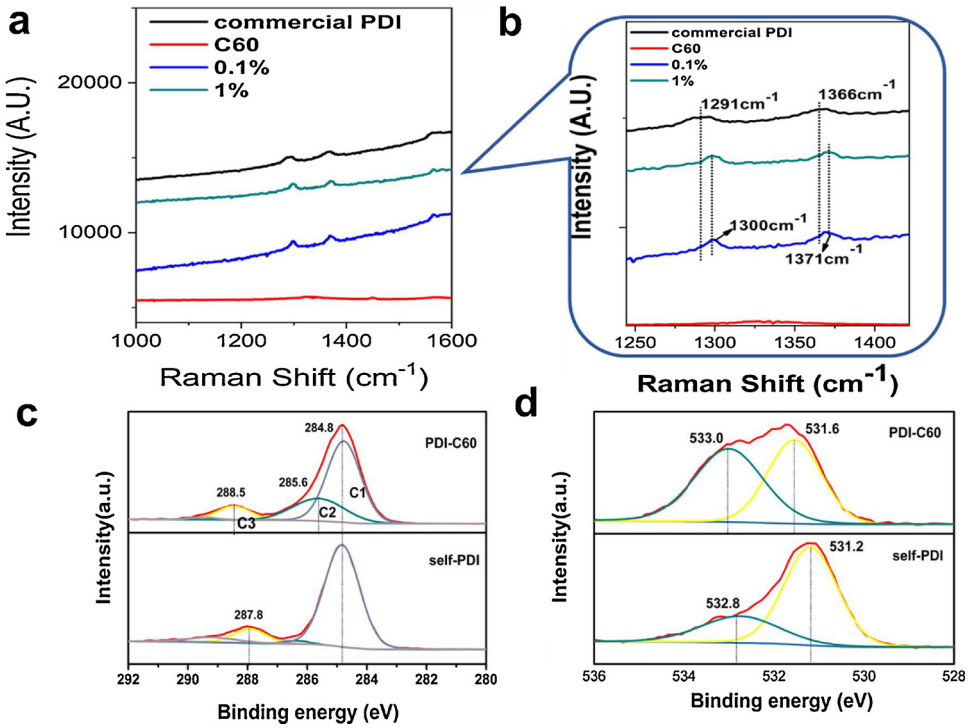

Fig. 4. Spectroscopy of PTCDI-C_{60} composites: (a) Raman spectra of PTCDI, 0.1%-PTCDI-C_{60}, and 1%-PTCDI-C_{60} and its enlarged drawing(b). High-resolution XPS spectra of self-assemble PTCDI and PTCDI-C_{60}-0.1% (c) C1s and (d) O1s.

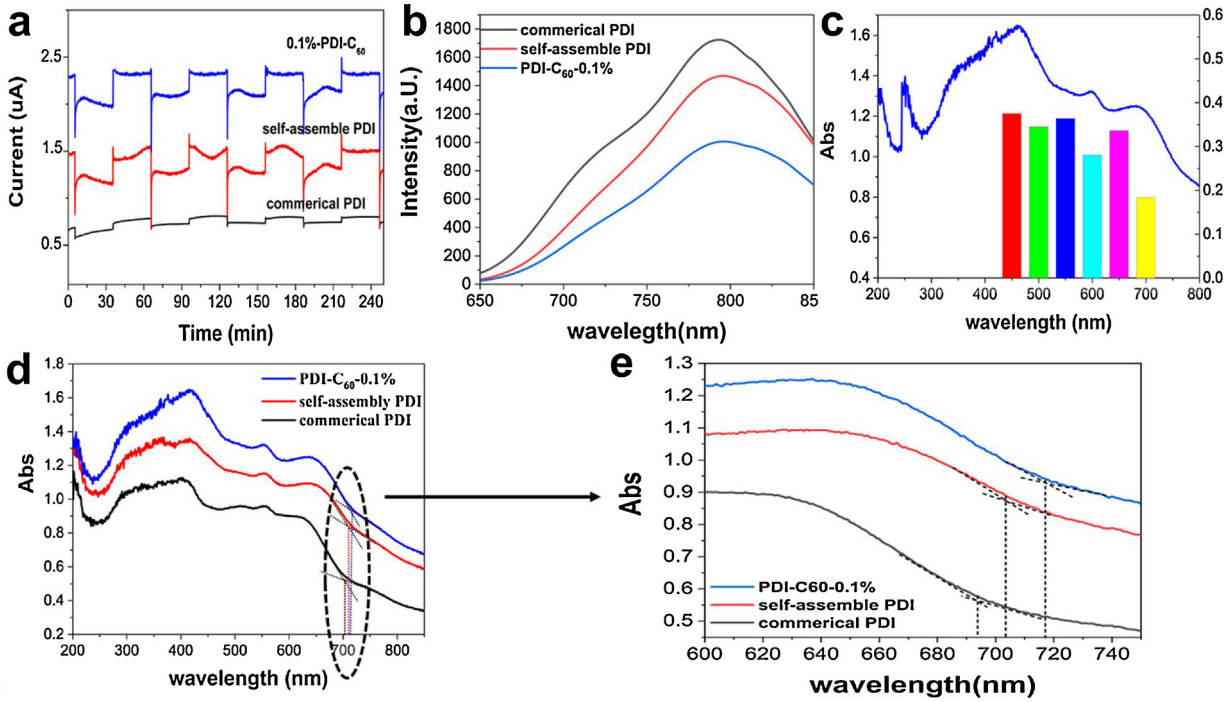

Fig. 5. (a) photocurrent spectra of pure PTCDI, self-assemble PDCDI and 0.1%-PTCDI-C_{60}. (b) fluorescence spectra of pure PTCDI, self-assemble PDCDI and 0.1%-PTCDI-C_{60}. (c) Absorbance and degradation rate constants k of 0.1%-PTCDI-C_{60}. (d)UV-DRS spectra of pure PTCDI, self-assemble PDCDI and 0.1%-PTCDI-C_{60} and its enlarged drawing(e).

and 0.1%-PTCDI-C_{60} supramolecular systems. Such hydrogen bond interactions together with intermolecular π–π stacking interactions are proposed to influence the arrangement of PTCDI molecules in 0.1%-PTCDI-C_{60} supramolecular system.

Raman scattering spectra of pure PTCDI, C_{60} and PTCDI-C_{60} samples are collected with the laser wavelength of 514 nm in order to minimize the effect of fluorescence effect (Fig. 4a and b). It is known that fullerene compounds with charge transfer exhibit significant line shifts in their Raman spectra. One of the most sensitive modes to charge transfer in C_{60} is the Ag (2) mode [32]. Raman spectra of PTCDI-C_{60} sample shows obvious change of the Ag (2) mode and this can be considered as reliable evidence for charge transfer in the composites. In the case of PTCDI-C_{60}, the peak of G band is broadened and the center of the peak shifts to a higher frequency from 1291 to 1300 cm^{-1}, from

1366 cm^{-1} to 1371 cm^{-1} compared to pure PTCDI. It is evidence of the presence of the electron transfer from self-assemble PTCDI to C_{60}, namely, a strong π-π interface interaction.

X-ray photoelectron spectroscopy (XPS) analysis was used to test the interaction between PTCDI and C_{60}. As shown in Fig. 4(c and d). The C1s spectra of PTCDI-C60-0.1% show three peaks at 284.8 (C1), 285.6 (C2), and 288.5 eV (C3). The peak at 284.8 eV represents the carbon contaminations. The dominant peak at 285.8 eV represents the sp2 hybridized carbon, which is combined to C, and the peak at 288.5 eV represents the sp2 hybridized carbon, which is combined to the -NH_2. The corresponding O 1 s spectrum of PTCDI-C_{60}-0.1% is divided into two main peaks: the presence of carbonyl O atoms at 531.4 eV and the acid anhydride O atoms at 533.0 eV. Interestingly, the binding energy of both C 2 s and O 2 s in PTCDI-C_{60}-0.1% exhibit obvious increase compared with self-assemble PTCDI, proving that the chemical states of both carbon and oxygen were changed and there may be strong interaction of conjugative π -bond between self-assemble PTCDI and C_{60}, which could improve the charge separation efficiency in the system [33].

3.3. Mechanism of enhancing photocatalytic activity

In the UV-DRS spectra (Fig. 5d), the absorption of 0.1%-PTCDI-C_{60} in the visible range was extended by about 20 nm and 10 nm respectively in comparison with pure PTCDI and self-assemble PTCDI. The band structure for charge migration and separation could be optimized, indicating band narrowing of ~0.07 eV. The band-edge shift is significant because, in this case, electrons can be stimulated under lower-energy irradiation, making full use of the whole spectrum in comparison to UV photocatalysts. Meanwhile, the lower the excitation energy, the less photocorrosion occurs.

In order to understand the mechanism of PTCDI-C_{60} thoroughly, investigation into the factors influencing the photocatalytic activity of PTCDI-C_{60} supramolecular system is essential.

As showed in Fig. 5a, the 0.1%-PTCDI-C_{60} supramolecular system exhibits higher photocurrent response than pure PTCDI and self-assemble PTCDI under irradiation of visible light, suggesting a great separation and transport ability of photocarriers, in other words, a lower probability of recombination of photogenerated carriers in the 0.1%-PTCDI-C_{60} composites can be confirmed. The fluorescence emission of 0.1%-PTCDI-C_{60} supramolecular system showed a significant reduction (Fig. 5b). This phenomenon reflected low recombination probability of photo induced carriers in 0.1%-PTCDI-C_{60}. The photo-generated electrons of PTCDI-C_{60} prefer to migrate along the π–π long-range transport pathway through charge delocalization, then, the electron is passed through the large π bond of C_{60}. By this way, recombination probability of photo induced carriers will be inhibited. The wavelength dependent photodegradation results show that the photodegradation rate constants (k) can be related to optical absorption as a function of wavelength (Fig. 5c). The trends of phenol degradation rates of the 0.1%-PTCDI-C_{60} supramolecular system along with the wavelengths match well with its optical absorption curve, indicating that the optical absorption may contribute a lot to its photodegradation performance.

Although C_{60} is an excellent electron-transferring material and beneficial for charge separation in the PTCDI-C_{60} photocatalyst. However, too much C_{60} will also shade PTCDI, leading to less photon absorption and a lower quantum yield. Thus, there is a balance between charge separation and light absorption, where 0.1% of C_{60} by mass might represent the balance point. At less than 0.1%, C_{60} enhances the electron transport and induces the formation of nanocrystals of PTCDI, resulting in an increased catalytic activity; on the contrary, more than 0.1%, C_{60} shades PTCDI, and reduces the number of photogenerated electrons and holes, resulting in a decrease of catalytic activity.

The processes of phenol degradation and intermediate formation were investigated by high-performance liquid chromatography (HPLC) (Fig. 6e). The peak at 3.557 min represents phenol, the intensity decreased after 6 h of irradiation as a result of the photocatalytic reaction. It can be seen that phenol was completely mineralized.

Fig. 6d shows the photodegradation of phenol in the presence of hole scavengers (formic acid), a hydroxyl radical scavenger (t-BuOH), a superoxide radical scavenger (P-benzoquinone) and an electron scavenger ($AgNO_3$) under visible light. The photocatalytic activity of 0.1%-PTCDI-C_{60} decreased to diff ;erent extents in the several diff ;erent cases, for example, formic acid, P-benzoquinone and t-BuOH, which implies that holes, superoxide radicals and a small hydroxyl radical contribute to the photocatalytic reaction. However, the activity of the composite increased when an electron scavenger, $AgNO_3$, was added, which resulted from the increase of the superoxide radical. The reason is the same as the mechanism of the water oxidation process following will be explained.

Further, the ESR detection of in situ active species (Fig. 6a, b, c) indicated that both $^1O_2$, $\cdot O_2^-$ and e^- which also contribute to the photocatalytic oxidation, could be detected after irradiation. In short, $^1O_2$, and $\cdot O_2^-$ are the main active species and govern the photocatalytic oxidation process. Moreover, photogenerated electrons are transferred along the π–π long-range transport pathway to dissolved oxygen through C_{60}, and then the dissolved oxygen gains electrons, changing into $\cdot O_2^-$ to oxidize the phenol.

The electronic energy level structure of PTCDI-C_{60} and self-assembled PTCDI supramolecular system was investigated by combining Mott–Schottky (MS) measurements with X-ray photoemission spectroscopy (XPS) valence band spectra. The flat-band potential obtained from the χ intercepts of the linear region in MS plots was found to be −1.0 V versus SCE and -1.1 V versus SCE (Fig. S5). It was reported that the conduction bands of n-type semiconductors are normally 0.1 − 0.2 eV deeper than the flat band potential [34]. Herein, the voltage differences between CB value and the flat potential value are set to be 0.1 eV, and thus the bottom of the conduction band is estimated to be −0.655 eV versus NHE and −0.755 eV versus NHE, which is more positive than the LUMO level (−0.92 eV) of monomeric PTCDI.

The XPS valence band spectrum of pure PTCDI, self-assembled PTCDI and PTCDI-C_{60} supramolecular system reveals the VB position at about 1.33 eV, 1.49 eV and 1.7 eV respectively. Deeper VB position (+1.7 eV) gives rise to thermodynamic driving force of PTCDI-C_{60} supramolecular system for O_2 evolution. Upon visible light irradiation, photo-generated electrons prefer to migrate along the long-range transport pathway through charge delocalization.

Based on the above results, the mechanism of photocatalytic reaction was depicted in Fig. 7. Upon visible light irradiation, photo-generated electrons prefer to migrate along the π–π long-range transport pathway and tend to transfer to C_{60} particles due to their excellent electronic conductivity, then through charge delocalization, while holes can easily spread out over PTCDI-C_{60} supramolecular system with nanoscale thickness to catch pollutants or oxide water, leading to effective spatial charge separation.

The progress of the water oxidation process can be explained by the following three reactions.

$$Ag^+ + H_2O \rightarrow Ag^\circ + H^+ + O_2 \quad (1)$$

$$C_{60} + H_2O \rightarrow C_{60}^- + H^+ + O_2 \quad (2)$$

$$PTCDI + H_2O \rightarrow PTCDI^- + H^+ + O_2 \quad (3)$$

Eq. (1) presents the overall reaction in the photocatalytic process. The rate declines gradually after long-time irradiation, as a result of the consumption of silver nitrate. In the presence of C_{60}, photogenerated charge carriers are separated and transferred rapidly: photoinduced electrons are transferred to Ag^+ by C_{60}, and more holes are left in PTCDI to oxidize water. Under these conditions, with a decrease in Ag^+, the photoinduced electrons cannot be depleted. As the reaction proceeds, because of their high electron affinities, C_{60} and PTCDI are transformed into C_{60}^- and $PTCDI^-$ anions (Eqs. (2) and (3)), which

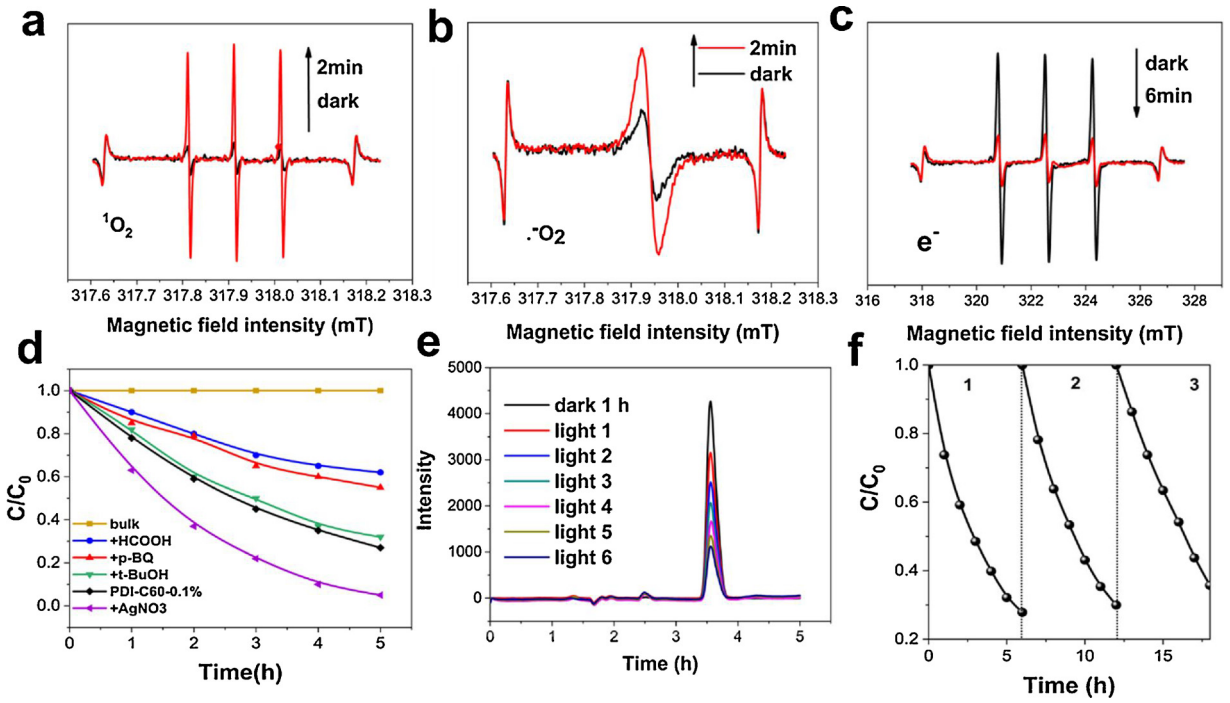

Fig. 6. (a) ESR detection of -O_2. (b) ESR detection of $^1O_2$. (c) ESR detection of e^-. (d) photodegradation of phenol in the presence of scavengers. (e)HPLC map of initial 5 ppm phenol to the map of phenol after 6 h of photocatalytic degradation. (f) Cyclic experiments using 0.1%-PTCDI-C_{60} for phenol (5 ppm) degradation.

gradually accumulate, leading to a collapse of the π–π stacking. As a result, the rate of oxygen evolution decreases.

The stability of PTCDI-C_{60} was tested by repeated cycling experiments. As shown in Fig. 6f, the photocatalyst exhibited excellent stability. The cyclic of photodegradation 5 ppm phenol was carried out 3 times, and 6 h each time. After each cycle, we centrifuged the solution to separate out the photocatalyst; however, because of its nanoscale size and excellent dispersibility in water, there was always a large amount of photocatalyst that did not completely settle, resulting in a loss of photocatalyst. However, the subsequent three cycles exhibited similar reaction rates, thus confirming the cycling performance and stability of the photocatalyst for application in photodegradation.

4. Conclusion

A highly efficient PTCDI-C_{60} composite photocatalyst was synthesized by a solution-based self-assembly route and π–π interactions. The π–π stacking of self-assembled PTCDI and π–π interactions between self-assembled PTCDI and C_{60} play a significant role in accelerating charge transfer, not only decreasing the recombination of photogenerated electron–hole pairs but also deepening the VB position. The composite photocatalyst with the mass ratio of C_{60} reached 0.1% was found to have the highest activity, which was 8.24 times that of pure PTCDI for the degradation of organic pollutants, and to generate oxygen at a rate of 22.5 μmol g^{-1} h^{-1}. The composite material has good stability. With its potential in environmental treatment and clean energy production, 0.1%-PTCDI-C_{60} might be a promising photocatalyst in the near future.

Acknowledgements

This work was partly supported Chinese National Science Foundation (21437003, 21673126, 21761142017, 21621003) and Collaborative Innovation Center for Regional Environmental Quality.

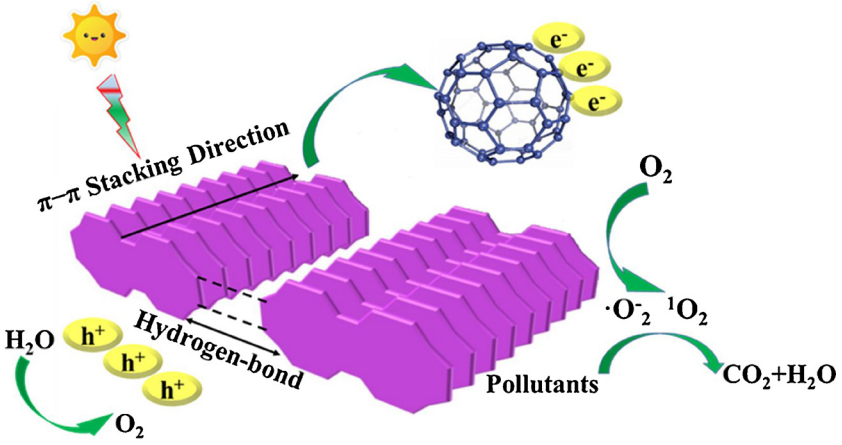

Fig. 7. schematic of the mechanism of photocatalytic oxidation.

Appendix A. Supplementary data

Supplementary material related to this article can be found, in the online version, at doi:https://doi.org/10.1016/j.apcatb.2018.07.043.

References

[1] N. Serpone, A.V. Emeline, Semiconductor photocatalysis - past, present, and future outlook, J. Phys. Chem. Lett. 3 (2012) 673–677.
[2] C.A. Hunter, J.K.M. Sanders, The nature of tt-tt interactions, J. Am. Chem. Soc. 112 (1990) 5525–5534.
[3] S.K. Burley, G.A. Petsko, Aromatic-aromatic interaction: a mechanism of protein structure stabilization, Science 229 (1985) 23–28.
[4] C.A. Hunter, J. Singh, J.M. Thornton, π-π interactions: the geometry and energetics of phenylalanine-phenylalanine interactions in proteins, J. Mol. Biol. 218 (1991) 837–846.
[5] E.A. Meyer, R.K. Castellano, F. Diederich, Interactions with aromatic rings in chemical and biological recognition, Angew. Chem. Int. Edit. 42 (2003) 1210–1250.
[6] C.G. Claessens, J.F. Stoddart, π–π interactions in self-assembly, J. Phys. Org. Chem. 10 (1997) 254–272.
[7] J. Wang, D. Liu, Y.F. Zhu, S.Y. Zhou, S.Y. Guan, Supramolecular packing dominant photocatalytic oxidation and anticancer performance of PDI, Appl. Catal. B 231 (2018) 251–261.
[8] B. Askew, P. Ballester, C. Buhr, K.S. Jeong, S. Jones, K. Parris, K. Williams, J. Rebek, Molecular recognition with convergent functional groups. 6. Synthetic and structural studies with a model receptor for nucleic acid components, J. Am. Chem. Soc. 111 (1989) 1082–1090.
[9] D.B. Smithrud, F. Diederich, Strength of molecular complexation of apolar solutes in water and in organic solvents is predictable by linear free energy relationships: a general model for solvation effects on apolar binding, J. Am. Chem. Soc. 112 (1990) 339–343.
[10] C.A. Hunter, The role of aromatic interactions in molecular recog n it ion, Chem. Soc. Rev. 23 (1994) 101–109.
[11] Rebek, Assembly and encapsulation with self-complementary molecules, J. Chem. Soc. Rev. 25 (1996) 255–264.
[12] P.T. Hammond, Form and function in multilayer assembly: new applications at the nanoscale, Adv. Mater. 16 (2004) 1271–1293.
[13] F. Würthner, C.R. Saha-Möller, B. Fimmel, S. Ogi, P. Leowanawat, D. Schmidt, Perylene bisimide dye assemblies as archetype functional supramolecular materials, Chem. Rev. 116 (2016) 962–1052.
[14] P.R.L. Malenfant, C.D. Dimitrakopoulos, J.D. Gelorme, L.L. Kosbar, T.O. Graham, A. Curioni, W. Andreoni, N-type organic thin-film transistor with high field-effect mobility based on a N,N′N,N′-dialkyl-3,4,9,10-perylene tetracarboxylic diimide derivative, Appl. Phys. Lett. 80 (2002) 2517–2519.
[15] G. Horowitz, F. Kouki, P. Spearman, D. Fichou, C. Nogues, X. Pan, F. Garnier, Evidence for n-type conduction in a perylene tetracarboxylic diimide derivative, Adv. Mater. 8 (1996) 242–245.
[16] R.S. Loewe, R.K. Lammi, J.R. Diers, C. Kirmaier, D.F. Bocian, D. Holten, J.S. Lindsey, Design and synthesis of light-harvesting rods for intrinsic rectification of the migration of excited-state energy and ground-state holes, J. Mater. Chem. 12 (2002) 1530–1552.
[17] H. Wang, D. Wang, Q. Wang, X. Li, C.A. Schalley, Nickel(II) and iron(III) selective off-on-type fluorescence probes based on perylene tetracarboxylic diimide, Org. Biomol. Chem. 8 (2010) 1017–1026.
[18] H. Yu, P. Joo, D. Lee, B.S. Kim, J.H. Oh, Photoinduced charge-carrier dynamics of phototransistors based on perylene diimide/reduced graphene oxide core/Shell p–n junction nanowires, Adv. Opt. Mater. 3 (2015) 241–247.
[19] D. Liu, J. Wang, X.J. Bai, R.L. Zong, Y.F. Zhu, Self-assembled PDINH supramolecular system for photocatalysis under visible light, Adv. Mater. 28 (2016) 7284–7290.
[20] Z.J. Zhang, J. Wang, D. Liu, W.J. Luo, M. Zhang, W.J. Jiang, Y.F. Zhu, Highly efficient organic photocatalyst with full visible light spectrum through π-π stacking of TCNQ-PTCDI, Appl. Mater. Interfaces 8 (2016) 30225–30231.
[21] T. Hasobe, S. Hattori, P.V. Kamat, S. Fukuzumi, Supramolecular nanostructured assemblies of different types of porphyrins with fullerene using TiO_2 nanoparticles for light energy conversion, Tetrahedron 62 (2006) 1937–1946.
[22] G. Yu, J. Gao, J.C. Hummelen, F. Wudl, A.J. Heeger, Polymer photovoltaic cells: enhanced efficiencies via a network of internal donor-acceptor heterojunctions, Science 270 (1995) 1789–1791.
[23] P.V. Kamat, M. Gevaert, K. Vinodgopal, Photochemistry on semiconductor surfaces. Visible light induced oxidation of C_{60} on TiO_2 nanoparticles, J. Phys. Chem. B 101 (1997) 4422–4427.
[24] T. Hasobe, H. Imahori, S. Fukuzumi, P.V. Kamat, Light energy conversion using mixed molecular nanoclusters. Porphyrin and C_{60} cluster films for efficient photocurrent generation, J. Phys. Chem. B 107 (2003) 12105–12112.
[25] H.B. Fu, T.G. Xu, S.B. Zhu, Y.F. Zhu, Photocorrosion inhibition and enhancement of photocatalytic activity for ZnO via hybridization with C_{60}, Environ. Sci. Technol. 42 (2008) 8064–8069.
[26] Y.Z. Long, Y. Lu, Y. Huang, Y.C. Peng, Y.J. Lu, S.Z. Kang, J. Mu, Effect of C_{60} on the photocatalytic activity of TiO_2 nanorods, J. Phys. Chem. C 113 (2009) 13899–13905.
[27] S.B. Zhu, T.G. Xu, H.B. Fu, J.C. Zhao, Y.F. Zhu, Synergetic effect of Bi_2WO_6 photocatalyst with C_{60} and enhanced photoactivity under visible irradiation, Environ. Sci. Technol. 41 (2007) 6234–6239.
[28] Y.Y. Ma, H. Wang, J.L. Key, S. Ji, W.Z. Lv, R.F. Wang, Control of CuO nanocrystal morphology from ultrathin “willow-leaf” to “flower-shaped” for increased hydrazine oxidation activity, J. Power Sources 300 (2015) 344–350.
[29] J.J. Wei, J.J. Wang, J.Y. Zhou, R.C. Zhang, D.J. Zhang, Synthesis of $Zn_{0.3}Co_{2.7}O_4$ porous willow-leaf like structure for enhanced electrocatalytic oxygen evolution reaction, Mater. Lett. 198 (2017) 196–200.
[30] C.A. Hunter, The role of aromatic interactions in molecular recog n it ion, Chem. Soc. Rev. 23 (1994) 101–109.
[31] T.E. Kaiser, H. Wang, V. Stepanenko, F. Würthner, Supramolecular construction of fluorescent j-aggregates based on hydrogen-bonded perylene dyes, Angew. Chem. Int. Ed. 46 (2007) 5541–5544.
[32] D.S. Bethune, G. Meijer, W.C. Tang, H.J. Rosen, W.G. Golden, H. Seki, C.A. Brown, M.S. Devries, Vibrational Raman and infrared spectra of chromatographically separated C_{60} and C_{70} fullerene clusters, Chem. Phys. Lett. 179 (1991) 181–186.
[33] X.J. Bai, C.P. Sun, S.L. Wu, Y.F. Zhu, Enhancement of photocatalytic performance via a P3HT-g-$C3N_4$ heterojunction, J. Mater. Chem. A 3 (2015) 2741–2747.
[34] J.L. Wang, Y. Yu, L.Z. Zhang, Highly efficient photocatalytic removal of sodium pentachlorophenate with Bi_3O_4Br under visible light, Appl. Catal. B 136–137 (2013) 112–121.